

International Atomic Energy Agency

INDC(JPN)-118/L

**INDC**

**INTERNATIONAL NUCLEAR DATA COMMITTEE**

---

**MEASUREMENT AND ANALYSIS OF DOUBLE DIFFERENTIAL NEUTRON  
EMISSION CROSS SECTIONS AT  $E_n = 14.1$  MeV FOR  $^{93}\text{Nb}$  AND  $^{181}\text{Ta}$**

A. Takahashi, Y. Sasaki and H. Sugimoto

Department of Nuclear Engineering, Faculty of Engineering  
Osaka University  
Osaka, Japan

January 1989

---

**IAEA NUCLEAR DATA SECTION, WAGRAMERSTRASSE 5, A-1400 VIENNA**



**MEASUREMENT AND ANALYSIS OF DOUBLE DIFFERENTIAL NEUTRON  
EMISSION CROSS SECTIONS AT  $E_n = 14.1$  MeV FOR  $^{93}\text{Nb}$  AND  $^{181}\text{Ta}$**

**A. Takahashi, Y. Sasaki and H. Sugimoto**

**Department of Nuclear Engineering, Faculty of Engineering  
Osaka University  
Osaka, Japan**

**January 1989**

**Reproduced by the IAEA in Austria  
January 1989**

**89-00350**

Measurement and Analysis of Double Differential Neutron Emission Cross Sections at  $E_n = 14.1$  MeV for  $^{93}\text{Nb}$  and  $^{181}\text{Ta}$  \*)

Akito Takahashi, Yasuhiro Sasaki and Hisashi Sugimoto

Department of Nuclear Engineering, Faculty of Engineering  
Osaka University  
Yamadaoka 2-1, Suita, Osaka-565, Japan

Abstract

Double differential neutron emission cross sections (DDX) at  $E_n = 14.1$  MeV for  $^{93}\text{Nb}$  and  $^{181}\text{Ta}$  were measured using an 8.3 m TOF spectrometer for 16 angles between  $15^\circ$  and  $160^\circ$ . Angle-integrated neutron emission spectra and angle-differential cross sections for elastic and resolved discrete inelastic scatterings were reduced from measured DDX data. For theoretical analyses, calculations were done using the EGNASH code which treated preequilibrium and equilibrium particle emissions. Direct inelastic components were calculated with the DWUCK4 code incorporated with EGNASH. Good agreements were obtained between these calculations and the experiments. Comparison with the ENDF/B-IV data, however, showed significant discrepancies.

Keywords

neutron emission, DDX, 14.1 MeV,  $^{93}\text{Nb}$ ,  $^{181}\text{Ta}$ , TOF, angle-integrated spectra, EGNASH, direct, precompound, ENDF/B-IV, Kalbach-Mann systematics

1. Introduction

Within the framework of the IAEA Coordinated Research Program (CRP) on measurement and analysis of 14 MeV neutron-induced double differential neutron emission cross sections needed for fission and fusion reactor technology, the present work for  $^{93}\text{Nb}$  and  $^{181}\text{Ta}$  has been carried out at the OKTAVIAN facility of Osaka University. The working group report of IAEA<sup>1</sup> (chaired by Prof. H. Vonach) recommends 'For medium and heavy nuclei ( $A = 50 - 209$ ), double differential neutron emission cross section data at  $E_n = 14$  MeV can be explained by the assumption of contributions from direct, precompound and

---

\*) This work has been supported by IAEA under the Research Agreement No. 4884/CF.

compound nucleus reactions, however, different theoretical approaches for the direct and precompound part are possible. Therefore accurate measurements should be made for one nucleus at different incident neutron energies to check the theoretical models.' Taking this recommendation in mind, measurements of double differential neutron emission cross sections (DDX) at the 14.1 MeV incident energy were carried out using a high resolution TOF spectrometer<sup>2</sup> of OKTAVIAN. We selected <sup>93</sup>Nb and <sup>181</sup>Ta for scattering samples, because pure isotopic samples are available in nature and theoretical analysis is therefore relatively easy. Theoretical analyses on DDX were done using the EGNASH code<sup>3</sup> which treated contributions of direct, precompound (angular dependence by the Kalbach-Mann systematics) and compound process. The experimental results were compared with the ENDF/B-IV data<sup>4</sup> and the Pavlik-Vonach evaluation<sup>5</sup>.

The experimental method is briefly written in Section 2, and the calculations by EGNASH in Section 3 and results with discussions in Section 4 are given.

## 2. Experimental

Description of the experimental method is given in detail elsewhere<sup>2</sup>. The pulsed D-T neutron source of OKTAVIAN was operated with 2 ns pulse width and 1 MHz repetition frequency. A cylindrical Nb or Ta metal sample with 3 cm in diameter and 7 cm long was set up at 17 cm distance radially apart from the tritium target, keeping the cylinder axis parallel to the deuteron beam line, as shown in Fig.1. Emitted neutrons from the sample were detected with an NE-213 liquid scintillator of 25.4 cm in diameter and 10 cm thick which located at 8.3 m distance from the tritium target. To change scattering angle, the sample was rotated around the tritium target and along the 17 cm radius arc. Since the collimator-shield assembly of TOF spectrometer was fixed in the 85° line against the deuteron beam line, incident neutron energy was 14.1 MeV with very slight ( $\pm 0.1$  MeV) variation according to the change of scattering angle which was within the energy resolution ( $\pm 0.2$  MeV) of the overall measuring system<sup>2</sup>.

The detail of the measuring system electronics, the neutron-gamma ray separability in pulse shape discrimination and the determination of energy-dependent detector efficiency is described elsewhere<sup>2</sup>. The neutron TOF analysis was done for the energy range of 0.5 - 14 MeV. The background time spectrum was taken by removing the cylindrical sample on a paper pipe support. The calibration of DDX data to obtain absolute values was undertaken using a hydrogen (polyethylene sample) elastic scattering at 25° in the laboratory angle. Double differential data were measured for 16 angle-points, i. e., 15°,

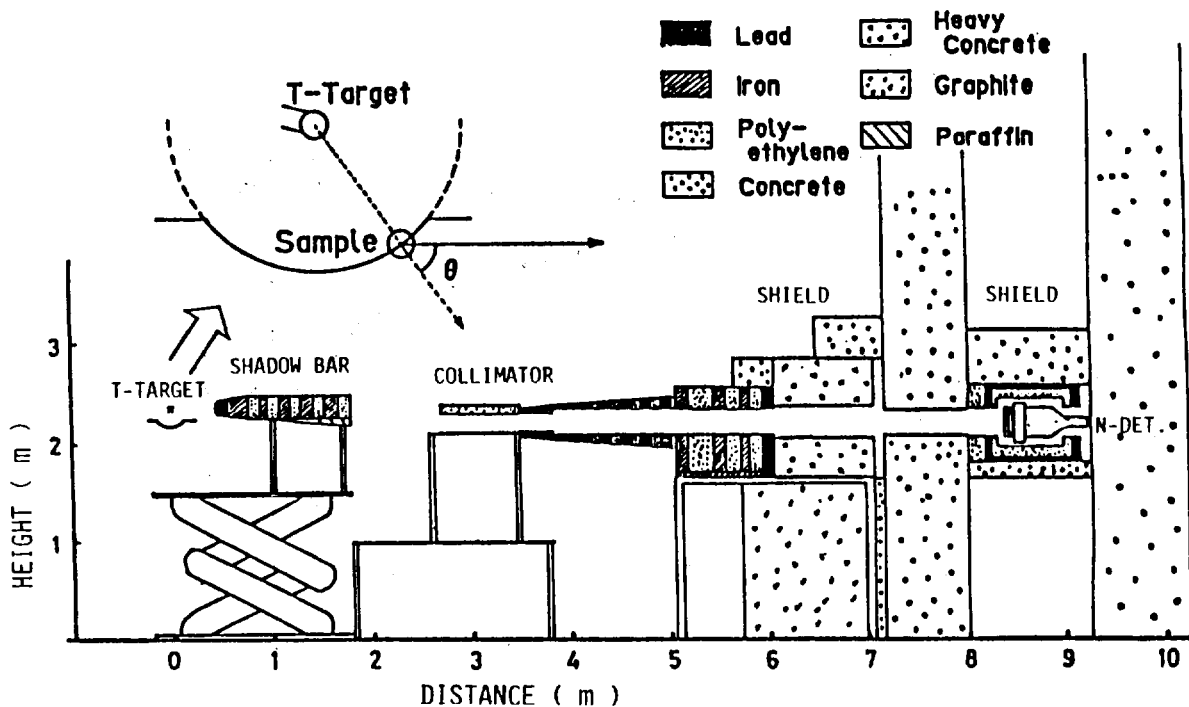


Fig.1 Layout of the TOF spectrometer with fixed incident neutron energy of 14.1 MeV

$20^\circ$ ,  $30^\circ$ ,  $40^\circ$ ,  $50^\circ$ ,  $60^\circ$ ,  $70^\circ$ ,  $80^\circ$ ,  $90^\circ$ ,  $100^\circ$ ,  $110^\circ$ ,  $120^\circ$ ,  $130^\circ$ ,  $140^\circ$ ,  $150^\circ$  and  $160^\circ$ , in the laboratory system. The detector efficiency is shown in Fig.2a.

The multiple scattering correction for raw DDX data was done using the MUSCC3 code<sup>6</sup> with the 135-group DDX-type data set generated from the ENDF/B-IV data<sup>4</sup>. Calculated correction factors were around unity within 10 % (at most) deviations for most of energy-bins (0.2 MeV width), except for backward elastic scattering peaks for which corrections were as large as about 30 %. The correction for the parasitic low energy tail of the source D-T neutron spectrum<sup>2</sup> was included in the MUSCC3 code and was found to be very small for most of scattering angles, except  $15^\circ$  and  $20^\circ$  at which the forward peaking of elastic scatterings by either Nb or Ta was effective for the low energy parasitic neutrons. The source neutron spectrum is shown in Fig.2b.

Angle-integrated neutron emission spectra (EDX) for  $^{93}\text{Nb}$  and  $^{181}\text{Ta}$  were reduced by integrating DDX data in the center-of-mass system which were converted from the LAB-angle DDX data using the kinematics of inelastic scatterings with pseudo-discrete levels of 0.0 – 14 MeV with 0.2 MeV interval<sup>7</sup>. Angle-differential cross sections (ADX) for resolved discrete excited states in the measured DDX data were deduced by calculating peak area within the energy bins that were specified with the energy resolution of the present experiment ( $\pm 0.2$  MeV). Results of DDX, EDX and ADX will be shown later, in comparison with the ENDF/B-IV data<sup>4</sup> and the theoretical calculations by EGNASH<sup>3</sup>. Numerical data tables of DDX will be given in the OKTAVIAN Report series from

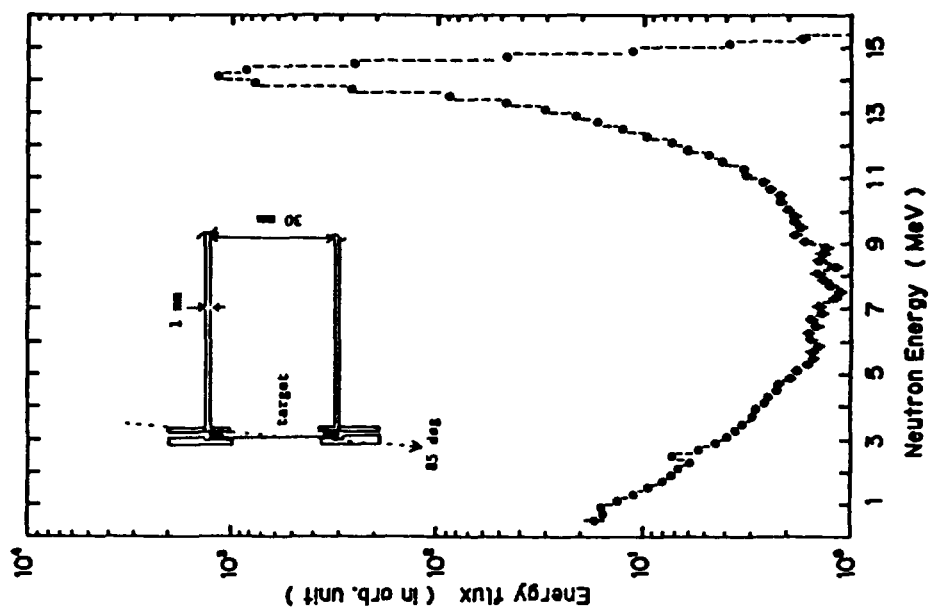


Fig. 2b Measured source neutron spectrum

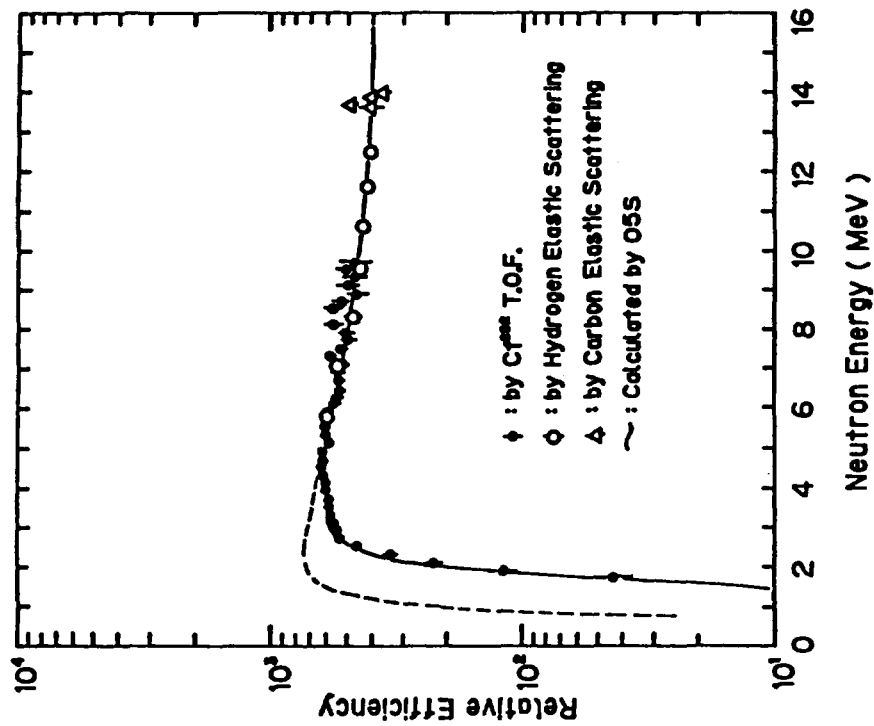


Fig. 2a Relative detector efficiencies ;  
solid line for high threshold,  
broken line for low threshold

Osaka University. However, numerical data of EDX and ADX are given later in this report.

For experimental errors, only statistical ones are shown in the following graphs and tables. To estimate overall errors, about 3 % error in every energy bin from efficiency calibration should be included.

### 3. Theoretical Analyses by EGNASH

The EGNASH code<sup>3</sup>, joint program of ELIESE and GNASH, developed by N. Yamamuro was used in the present analyses. In this joint code, double differential particle emission cross sections can be calculated using the output of DWUCK4<sup>8</sup> for direct reaction processes exciting isolated low-lying states of nucleus and the systematics of Kalbach and Mann<sup>9</sup> for preequilibrium (precompound) and equilibrium (compound) processes<sup>3</sup>. So, this is a similar approach to that used in the SMD/SMC theory analysis for <sup>93</sup>Nb by Kalka and Seeliger<sup>10</sup>. An input data set is given in the EGNASH code for the global optical model potential parameters by Walter and Guss<sup>11</sup>, the discrete level data from the Evaluated Nuclear Data Structure File (ENSDF) and parameters for the Fermi gas level density (continuous level). Other variables or parameters are set at the defaulted values or calculated in the program.

Calculation of the single-step direct inelastic scatterings by DWUCK4 was done only for <sup>93</sup>Nb, since the discrete level data for <sup>181</sup>Ta in ENSDF are limited to be less than 1.5 MeV in excitation energy and not sufficient for the present analysis. For <sup>93</sup>Nb, 27 discrete levels from 0.744 to 4.244 MeV were used with deformation parameters  $\beta_\lambda$  around 0.11, as shown in Table-1.

For the continuum particle emission spectra by the multistep direct (MSD, precompound) and multistep compound (MSC) processes, double differential cross section is written as<sup>9,12</sup>

$$\frac{d^2\sigma}{d\Omega d\epsilon}(a, b) = a_{\text{MSD}}(\text{MSD}) \sum_{\ell=0}^{\ell_{\text{max}}} b_{\ell} P_{\ell}(\cos\theta) + a_{\text{MSC}}(\text{MSC}) \sum_{\substack{\ell=0 \\ \Delta\ell=2}}^{\ell_{\text{max}}} b_{\ell} P_{\ell}(\cos\theta) \quad (1)$$

where only the even order polynomials contribute to the MSC part<sup>9,12</sup>.

By the assumption of Kalbach and Mann<sup>9</sup>,

$$b_{\ell}(\epsilon) = \frac{(2\ell+1)}{1 + \exp[A_{\ell}(B_{\ell} - \epsilon)]} \quad (2)$$

and they have given

$$A_{\ell} = 0.036 + 0.0039\ell(\ell+1), \text{ in MeV}^{-1} \quad (3a)$$

$$B_{\ell} = 92 - 90(\ell(\ell+1))^{-1/2}, \text{ in MeV} \quad (3b)$$

Table-1  
Input Parameters of Niobium for DWUCKY & EGNASH

E Level (MeV)	Spin	$\beta_L$	X-section at 14.1 MeV (barn)
0.7440	7/2	0.130	6.8532E-3
0.8087	5/2	0.120	5.1352E-3
0.9499	13/2	0.105	6.8341E-3
0.9789	11/2	0.105	6.2617E-3
1.0826	9/2	0.110	7.7930E-3
1.2973	9/2	0.110	8.5098E-3
1.3959	5/2	0.110	6.9037E-3
1.4834	7/2	0.110	4.9464E-3
1.4911	15/2	0.050	6.7328E-3
1.6035	9/2	0.110	6.1656E-3
1.6656	5/2	0.120	4.3959E-3
1.7101	5/2	0.120	4.3910E-3
1.9464	7/2	0.120	5.8177E-3
1.9687	11/2	0.115	8.0094E-3
2.1770	5/2	0.120	4.3334E-3
2.2036	9/2	0.115	6.0638E-3
2.3301	5/2	0.110	3.6235E-3
2.3673	9/2	0.110	5.4959E-3
2.4842	11/2	0.120	6.5689E-3
2.5862	5/2	0.120	3.5918E-3
2.8100	7/2	0.120	5.6521E-3
2.9800	5/2	0.120	4.2106E-3
3.1500	7/2	0.120	5.5745E-3
3.3000	7/2	0.115	5.0859E-3
3.5120	9/2	0.115	6.2943E-3
3.7200	11/2	0.110	6.8357E-3
4.2240	11/2	0.100	5.5503E-3

Table-2

Level Density Parameters of Niobium for EGNASH

Nucleus	a (MeV <sup>-1</sup> )	$\Delta$ (MeV)	T (MeV)
<sup>94</sup> Nb	14.0	0.00	0.746
<sup>93</sup> Nb	13.0	0.72	0.834
<sup>92</sup> Nb	11.5	0.00	0.790
<sup>91</sup> Nb	11.0	0.93	0.895
<sup>93</sup> Zr	13.7	1.20	0.781
<sup>92</sup> Zr	12.3	1.92	0.800
<sup>90</sup> Y	11.7	0.00	0.684
<sup>89</sup> Y	10.7	0.93	0.762

Level Density Parameters of Tantalum for EGNASH

Nucleus	a (MeV <sup>-1</sup> )	$\Delta$ (MeV)	T (MeV)
<sup>182</sup> Ta	23.8	0.00	0.470
<sup>181</sup> Ta	24.0	0.73	0.371
<sup>180</sup> Ta	24.5	0.00	0.453
<sup>179</sup> Ta	24.5	0.40	0.464
<sup>181</sup> Hf	24.5	0.64	0.441
<sup>180</sup> Hf	23.5	1.37	0.494
<sup>178</sup> Lu	24.4	0.00	0.329

Recently Kumabe et al<sup>1,2</sup> have given the following 'improved' coefficients.

$$A_\ell = 0.0561 + 0.0377 \ell \quad , \text{ in MeV}^{-1} \quad (4a)$$

$$B_\ell = 47.9 - 27.1 \ell^{-1/2} \quad , \text{ in MeV} \quad (4b)$$

In the present analyses, we tried both empirical presentations and will compare the results later.

The angle-integrated emission cross section (spectrum),  $a_0(\text{MSD}) + a_0(\text{MSC})$ , is calculated in the EGNASH code. For the optical model potential to calculate transition matrix for neutron, the Walter-Guss potential<sup>11</sup> was modified for the surface absorption term<sup>13</sup>. For charged particle emissions, the Perey, the Lemos and the Lohr-Haeaverli potential, respectively for p,  $\alpha$  and d are prepared<sup>13</sup> in the EGNASH code. Level density parameters used in the present analyses are tabulated in Table-2 and Table-3, respectively for Nb and Ta, where particle emissions are considered for (n,n'), (n,2n), (n,3n), (n,p), (n,np), (n,d), (n, $\alpha$ ) and (n,n' $\alpha$ ).

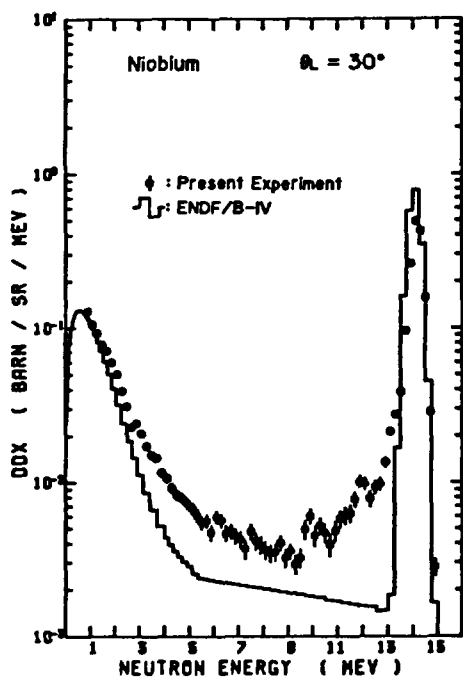
To compare with the experiment, calculated double differential cross sections were broadened using a Gaussian function with the experimental resolution  $1/\sigma = 0.3$  MeV that corresponds to 0.2 MeV in a half of FWHM.

#### 4. Results and Discussions

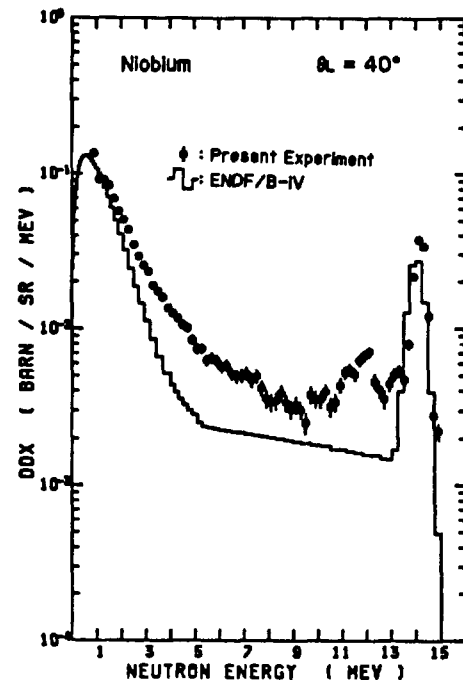
##### 4.1 Niobium

Double differential neutron emission cross sections (DDX): Measured double differential neutron emission cross sections in the laboratory system are shown for 8 angles, i. e.,  $30^\circ$ ,  $40^\circ$ ,  $60^\circ$ ,  $80^\circ$ ,  $100^\circ$ ,  $120^\circ$ ,  $140^\circ$  and  $160^\circ$ , in Fig.3a through Fig.3h where comparisons are made with the ENDF/B-IV data. In the high energy part of 9-13 MeV and below the elastic scattering peak, we can see 'structures' which presumably appear as a synthesis of many peaks by direct discrete inelastic scatterings. These direct reaction components of inelastic scatterings are not taken into account in the ENDF/B-IV data. In the lower energy region less than 9 MeV, the measured spectra look monotonous within error-bars and can be regarded as 'continuum'. Significant enhancement of neutron emission in forward angles is seen in the experimental 'continuum' spectra, which is in contrast with isotropic and softer spectral behavior of the ENDF/B-IV data.

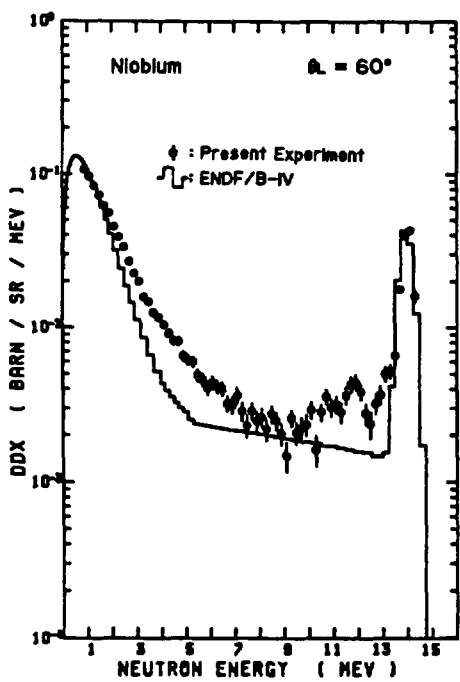
Calculated double differential cross sections in the center-of-mass system (CMS) by EGNASH are shown in Fig.4a through Fig.4d for 4 angles ( $30^\circ$ ,  $90^\circ$ ,  $140^\circ$  and  $150^\circ$ ), in comparison with experimental data which are also converted to CMS. Elastic scattering (right-most peaks in experimental DDX) is not included in the EGNASH calculation. In the continuum part (less than 9 MeV), the Kalbach-Mann



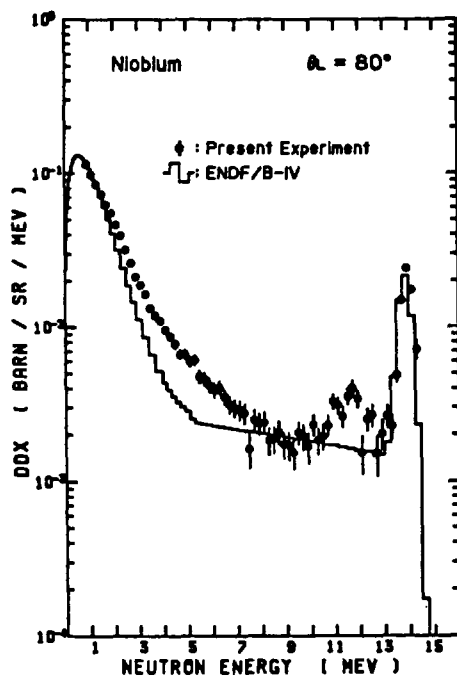
a)



b)

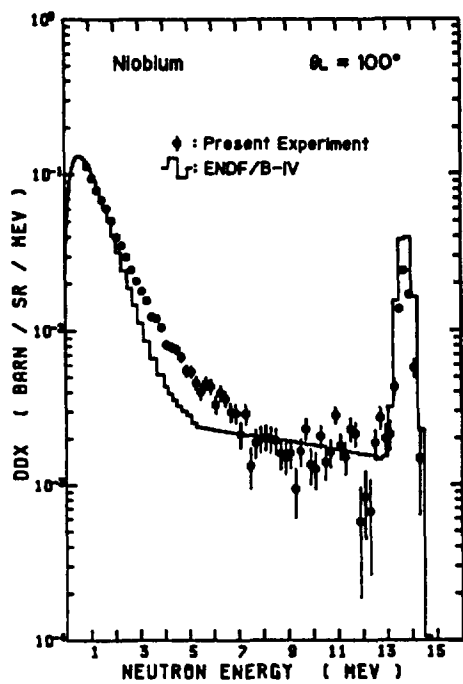


c)

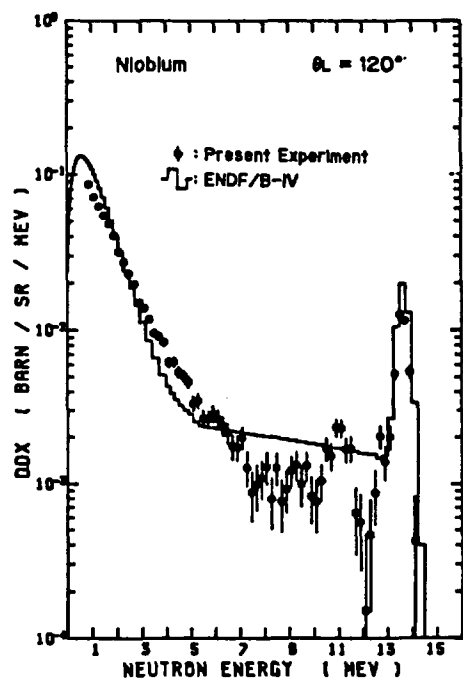


d)

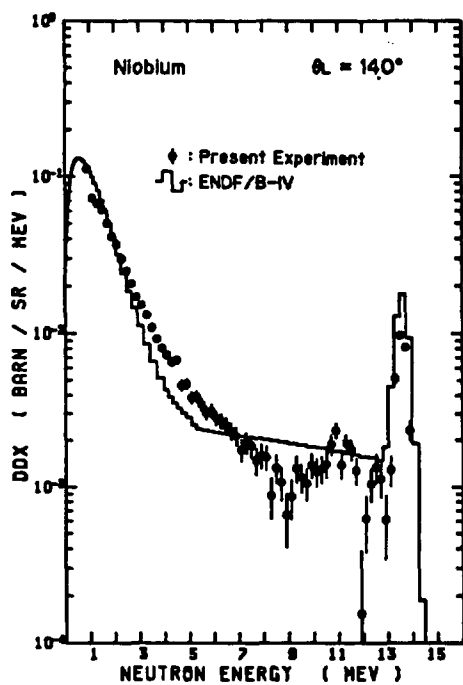
Figs. 3a-d      Double differential neutron emission cross sections at 14.1 MeV for Nb-93, in comparison with ENDF/B-IV



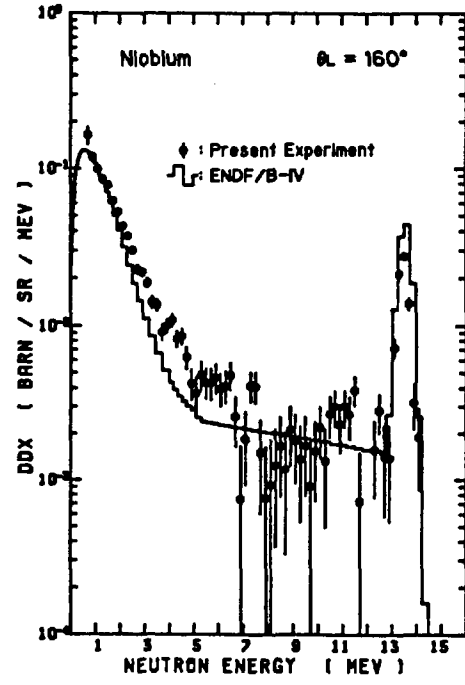
e)



f)

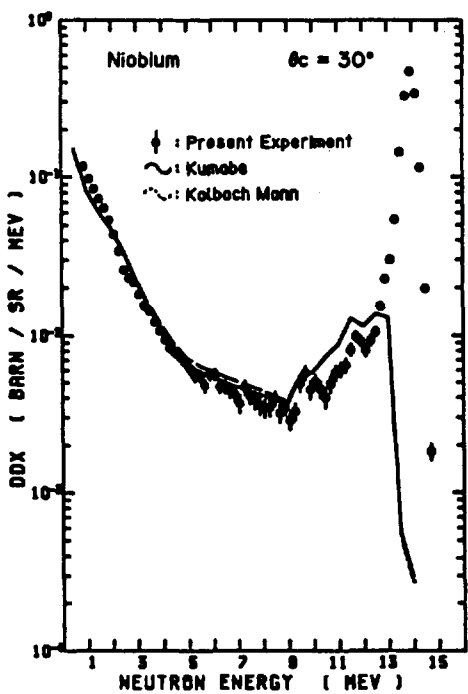


g)

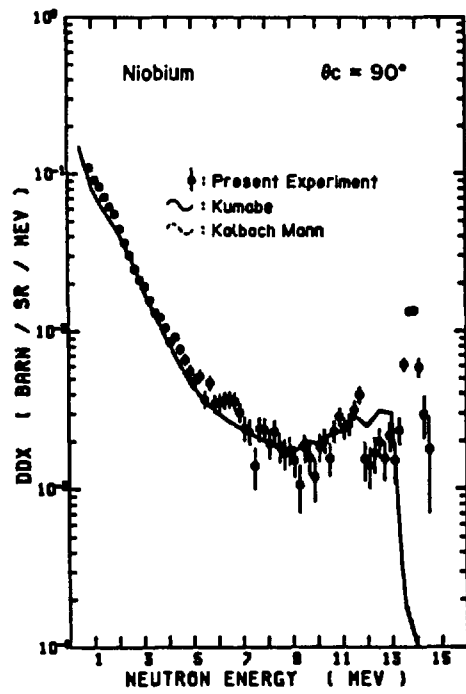


h)

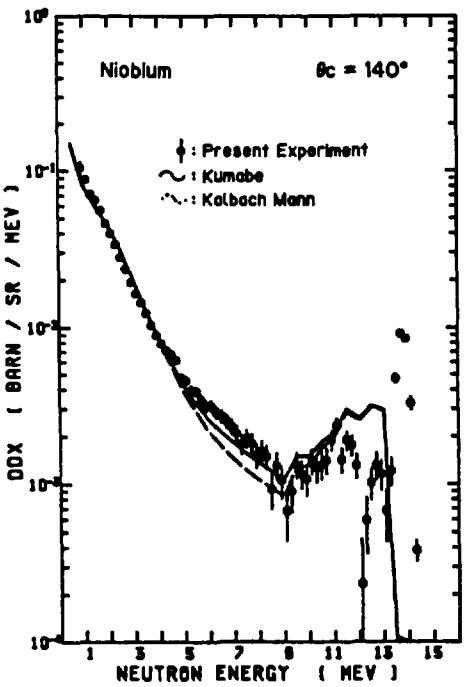
Figs. 3e-h Double differential neutron emission cross sections at 14.1 MeV for Nb-93, in comparison with ENDF/B-IV



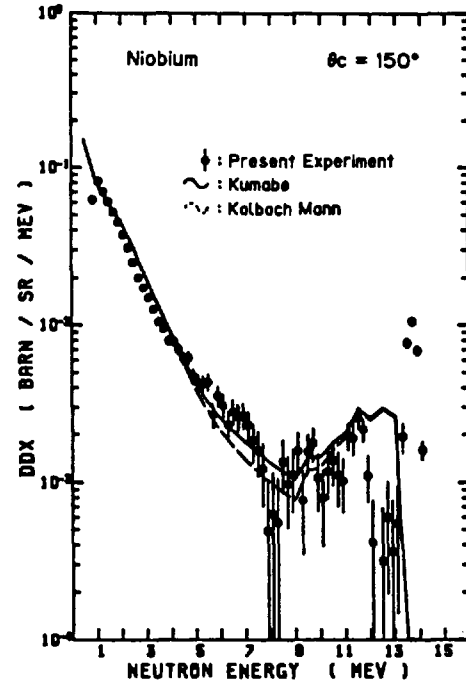
a)



b)



c)



d)

Figs. 4a-d Comparisons of double differential cross sections in CMS between experiments and calculations with EGNASH

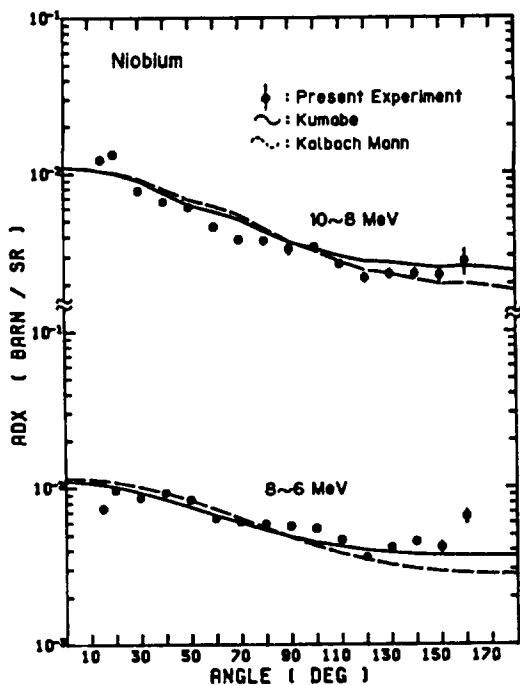
type statistics can well reproduce angular dependence of the present experimental data. The systematics of Kumabe et al<sup>12</sup> is more successful than that of Kalbach-Mann in forward ( $30^\circ$ ) and backward angles ( $140^\circ$  and  $150^\circ$ ), and can reproduce almost completely the experimental double differential data of the 'continuum' part. In the high energy region of 9-13 MeV, the calculation shows that the neutron emission by direct reaction process is dominant. In this energy region, the present calculation by DWUCK4 with the data of Table-1 can approximately reproduce the experimental spectral shape and magnitude in each angle, although significant overcalculations are seen at backward angles ( $140^\circ$  and  $150^\circ$ ) for excitation levels around 1 MeV, corresponding to 13 MeV of secondary neutron energy.

Angular differential cross sections (ADX) : To see angular dependency of the 'continuum' part, ADX data were reduced for artificial energy bins with 2 MeV width and are shown in Figs. 5a and 5b to be compared with the EGNASH calculations. The Kumabe systematics shows better agreement than the Kalbach-Mann's, for higher energy bins, i. e., 10-8, 8-6 and 6-4 MeV. For lower energy bins, 4-2 and 2-1 MeV, difference between the two empirical presentations is small and good agreement with the present experiment is seen although the experimental ADX data for the 2-1 MeV bin are about 10 % higher in average than the calculated values.

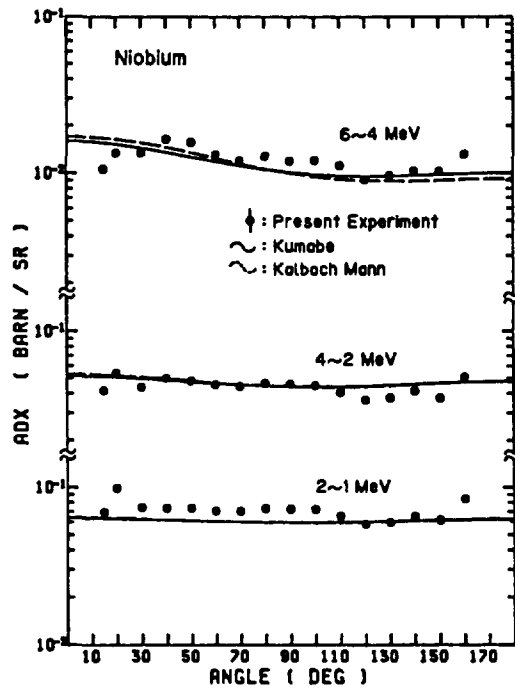
ADX data for 'resolved peaks' were reduced for the elastic, the '1.08 MeV state' and the sum-peak of '2.18-2.98 MeV states', and are shown in Figs. 6a and 6b. ADX data for the elastic scattering are shown in Fig.6a, in comparison with the ENDF/B-IV data which overestimates significantly in backward angles. For the inelastic ADX data of 1.08 and 2.18-2.98 MeV states, no comparison is made with the DWUCK4 calculation, however, we may compare using the proper bunching of so many (27) levels in the calculation. Kalka et al<sup>10</sup> used three discrete levels (0.93, 2.34 and 3.39 MeV states of  $^{92}\text{Zr}$ ) for their analysis of  $^{93}\text{Nb}(n,n')$  spectra. The presently reduced ADX data for the 1.08 and 2.18-2.98 MeV states may correspond to those of their 0.93 and 2.34 MeV states.

Numerical data of measured ADX are given in Table-4.

Angle-integrated neutron emission spectra (EDX) : Data in CMS are shown in Figs. 7a and 7b. In Fig.7a, the present experimental data are compared with the Pavlik-Vonach evaluation curve<sup>5</sup> (broken curve, evaluated with many experimental data upto 1987) and the ENDF/B-IV data (histgram). Being compared with the Pavlik-Vonach curve, the present experiment has given smaller (by about 15 % in average) emission cross sections in the 3-6 MeV region. Disagreement with the ENDF/B-IV spectrum is obvious in the 3-13 MeV region. The 'continuum'

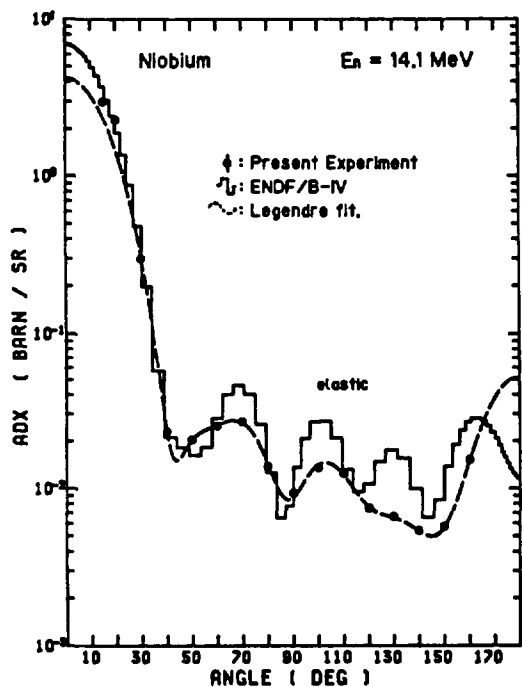


a)

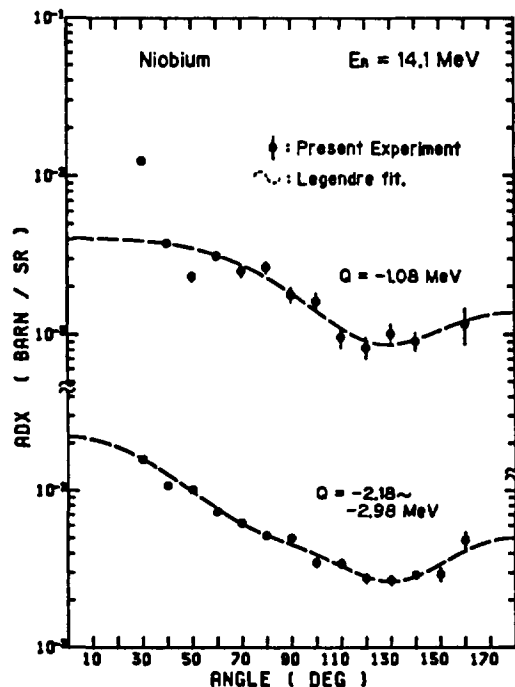


b)

Figs. 5a-b Angular distributions emitted neutrons for selected energy-bins, for Nb-93, compared with EGNASH calculations



a) elastic



b) resolved inelastic

Figs. 6a-b Angular differential cross sections of resolved levels, for Nb-93

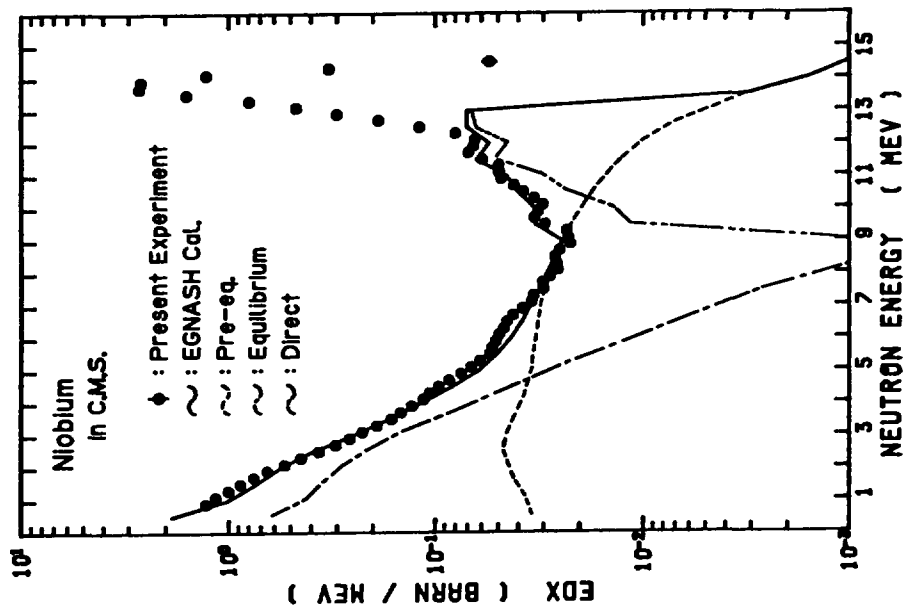


Fig. 7b Comparison of angle-integrated neutron emission spectra, for Nb-93, between experiment and EGNASH calculations

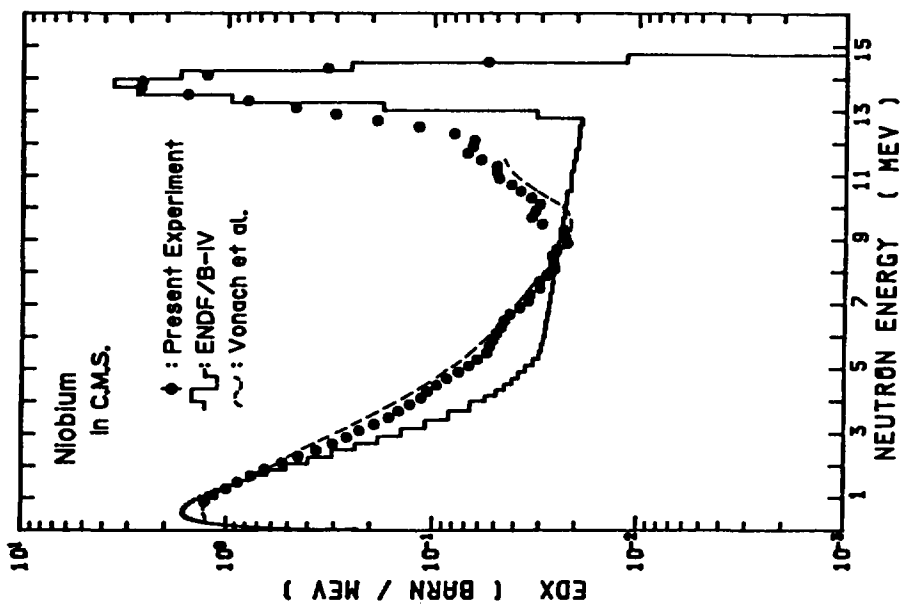


Fig. 7a Comparison of angle-integrated neutron emission spectra, for Nb-93, between experiment, ENDF/B-IV and Pavlik-Vonach evaluation

Table-4-1

Niobium partial differential cross sections at En=14.1MeV

Angle (deg)	elastic		Q=-1.08MeV		Q=-2.18~2.98MeV	
	dσ/dΩ (b/sr)	error (b/sr)	dσ/dΩ (b/sr)	error (b/sr)	dσ/dΩ (b/sr)	error (b/sr)
1. 500E+01	2. 996E+00	6. 607E-03				
2. 000E+01	2. 286E+00	4. 458E-03				
3. 000E+01	3. 006E-01	1. 464E-03	1. 246E-02	3. 670E-04	1. 585E-02	5. 112E-04
4. 000E+01	2. 305E-02	3. 633E-04	3. 787E-03	1. 544E-04	1. 079E-02	2. 832E-04
5. 000E+01	2. 043E-02	3. 923E-04	2. 325E-03	1. 437E-04	1. 013E-02	2. 956E-04
6. 000E+01	2. 513E-02	4. 889E-04	3. 142E-03	1. 830E-04	7. 301E-03	2. 692E-04
7. 000E+01	2. 679E-02	4. 985E-04	2. 517E-03	1. 918E-04	6. 221E-03	2. 597E-04
8. 000E+01	1. 392E-02	3. 598E-04	2. 659E-03	2. 000E-04	5. 191E-03	2. 293E-04
9. 000E+01	9. 371E-03	3. 914E-04	1. 774E-03	1. 801E-04	4. 996E-03	2. 414E-04
1. 000E+02	1. 361E-02	3. 665E-04	1. 616E-03	1. 850E-04	3. 503E-03	2. 210E-04
1. 100E+02	1. 244E-02	2. 775E-04	9. 635E-04	1. 365E-04	3. 455E-03	2. 086E-04
1. 200E+02	7. 479E-03	2. 069E-04	8. 276E-04	1. 221E-04	2. 774E-03	1. 768E-04
1. 300E+02	6. 627E-03	1. 975E-04	1. 012E-03	1. 363E-04	2. 690E-03	1. 725E-04
1. 400E+02	5. 402E-03	1. 595E-04	9. 079E-04	1. 100E-04	2. 917E-03	1. 511E-04
1. 500E+02	5. 738E-03	2. 718E-04			2. 948E-03	2. 715E-04
1. 600E+02	1. 526E-02	5. 792E-04	1. 161E-03	2. 837E-04	4. 848E-03	5. 400E-04

spectra (less than 9 MeV) by the present experiment and the Pavlik-Vonach evaluation are significantly hard, compared with the ENDF/B-IV spectrum.

In Fig.7b, calculated results with EGNASH are shown in comparison with the experimental EDX. The elastic scattering (right-most peak of the experimental spectrum) is not included in the calculation. The EGNASH calculation reproduces very well the experimental neutron emission spectrum. The calculated spectrum is composed of 4 components, i. e., the direct inelastic scattering (two-dotted line), the pre-equilibrium inelastic scattering (broken line), the first step equilibrium neutron emission (one-dotted line) and the second step equilibrium neutron emission (curve not drawn). In the 9-13 MeV region, the direct process plays a major role and partial cross sections to 27 discrete levels are given in Table-1. In the 4-9 MeV region, the preequilibrium process becomes dominant. In the lower energy region less than 4 MeV, neutrons from the equilibrium processes are dominant.

The present EGNASH calculation has been also checked for charged particle emissions. Results for proton and deuteron emissions are shown in Fig.8. For α-particle emission, result is shown in Fig.9. Agreements with experimental<sup>14</sup> data are satisfactory. Calculated <sup>93</sup>Nb(n,2n) and (n,3n) cross sections for various incident energies are shown in Fig.10, in comparison with experimental<sup>14</sup>

Table-4-2

Niobium integral of double differential cross section at En=14.1MeV

Angle (deg)	10-8 MeV		8-6 MeV		6-4 MeV	
	d $\sigma$ /d $\Omega$ (b/sr)	error (b/sr)	d $\sigma$ /d $\Omega$ (b/sr)	error (b/sr)	d $\sigma$ /d $\Omega$ (b/sr)	error (b/sr)
1. 500E+01	1. 223E-02	5. 929E-04	7. 362E-03	4. 076E-04	1. 059E-02	4. 657E-04
2. 000E+01	1. 320E-02	4. 223E-04	9. 595E-03	3. 256E-04	1. 344E-02	3. 322E-04
3. 000E+01	7. 761E-03	2. 887E-04	8. 687E-03	2. 871E-04	1. 345E-02	2. 784E-04
4. 000E+01	6. 608E-03	2. 235E-04	9. 312E-03	2. 226E-04	1. 631E-02	2. 272E-04
5. 000E+01	6. 096E-03	1. 848E-04	8. 355E-03	1. 950E-04	1. 562E-02	2. 179E-04
6. 000E+01	4. 575E-03	1. 534E-04	6. 395E-03	1. 673E-04	1. 300E-02	1. 973E-04
7. 000E+01	3. 819E-03	1. 535E-04	6. 067E-03	1. 745E-04	1. 198E-02	2. 043E-04
8. 000E+01	3. 765E-03	1. 826E-04	5. 874E-03	2. 068E-04	1. 279E-02	2. 400E-04
9. 000E+01	3. 340E-03	2. 224E-04	5. 698E-03	2. 527E-04	1. 187E-02	2. 838E-04
1. 000E+02	3. 422E-03	1. 778E-04	5. 503E-03	2. 078E-04	1. 199E-02	2. 454E-04
1. 100E+02	2. 693E-03	1. 436E-04	4. 634E-03	1. 689E-04	1. 110E-02	2. 048E-04
1. 200E+02	2. 195E-03	1. 300E-04	3. 590E-03	1. 452E-04	9. 083E-03	1. 708E-04
1. 300E+02	2. 324E-03	1. 451E-04	4. 154E-03	1. 545E-04	9. 660E-03	1. 702E-04
1. 400E+02	2. 320E-03	1. 515E-04	4. 534E-03	1. 517E-04	1. 031E-02	1. 591E-04
1. 500E+02	2. 272E-03	2. 917E-04	4. 187E-03	3. 121E-04	1. 023E-02	3. 112E-04
1. 600E+02	2. 780E-03	4. 935E-04	6. 577E-03	5. 731E-04	1. 309E-02	5. 393E-04

Angle (deg)	4-2 MeV		2-1 MeV	
	d $\sigma$ /d $\Omega$ (b/sr)	error (b/sr)	d $\sigma$ /d $\Omega$ (b/sr)	error (b/sr)
1. 500E+01	4. 179E-02	7. 638E-04	6. 923E-02	1. 457E-03
2. 000E+01	5. 381E-02	5. 010E-04	9. 873E-02	8. 618E-04
3. 000E+01	4. 386E-02	3. 592E-04	7. 444E-02	5. 820E-04
4. 000E+01	4. 971E-02	2. 919E-04	7. 359E-02	4. 668E-04
5. 000E+01	4. 779E-02	2. 904E-04	7. 361E-02	4. 421E-04
6. 000E+01	4. 547E-02	2. 990E-04	7. 073E-02	4. 640E-04
7. 000E+01	4. 448E-02	3. 251E-04	7. 044E-02	5. 085E-04
8. 000E+01	4. 630E-02	3. 686E-04	7. 329E-02	5. 655E-04
9. 000E+01	4. 574E-02	4. 120E-04	7. 260E-02	6. 084E-04
1. 000E+02	4. 472E-02	3. 600E-04	7. 223E-02	5. 524E-04
1. 100E+02	4. 066E-02	3. 054E-04	6. 547E-02	4. 849E-04
1. 200E+02	3. 653E-02	2. 585E-04	5. 845E-02	4. 227E-04
1. 300E+02	3. 751E-02	2. 478E-04	5. 986E-02	4. 136E-04
1. 400E+02	4. 143E-02	2. 220E-04	6. 523E-02	4. 727E-04
1. 500E+02	3. 743E-02	3. 834E-04	6. 194E-02	6. 554E-04
1. 600E+02	5. 065E-02	6. 375E-04	8. 447E-02	1. 042E-03

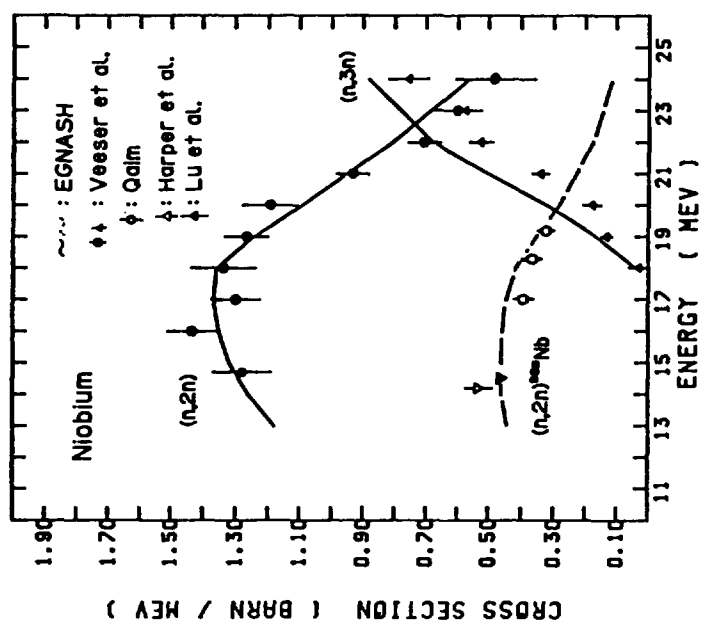


Fig.10 ( $n, 2n$ ) and ( $n, 3n$ ) cross sections for Nb-93, compared with EGNASH calculations

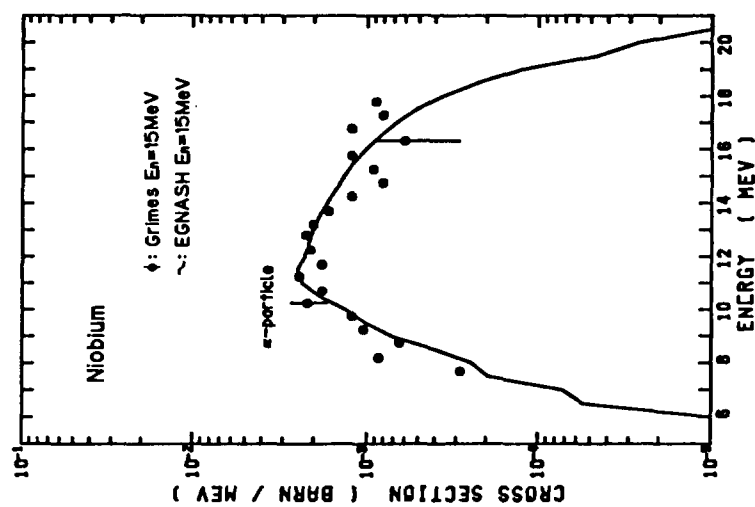


Fig.9 Alpha-particle spectra for Nb( $n, \alpha$ ), compared with EGNASH calculation

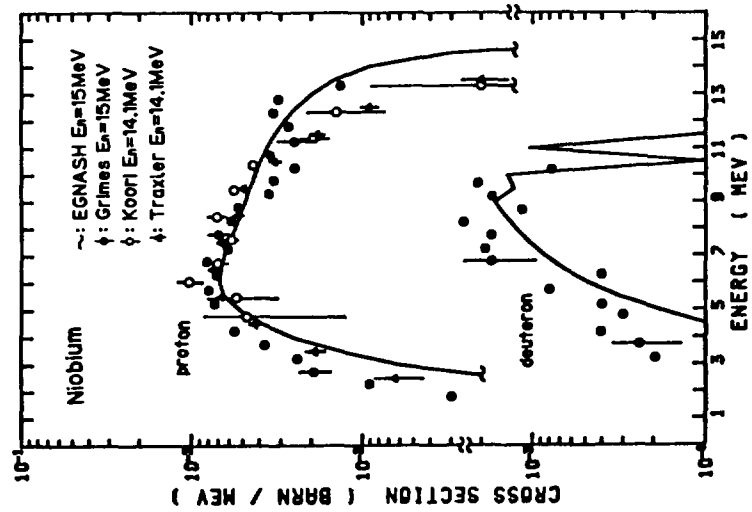


Fig.8 Charged-particle spectra for Nb( $n, p$ ) and Nb( $n, d$ ), compared with EGNASH calculations

Table-5

Niobium secondary neutron emission spectrum at En=14.1 MeV

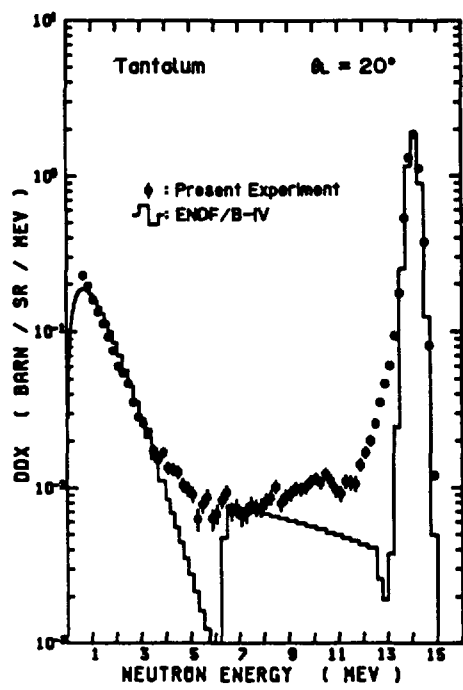
E-upper ( MeV )	E-lower ( MeV )	DATA ( Barn/MeV )	Error ( Barn/MeV )	E-upper ( MeV )	E-lower ( MeV )	DATA ( Barn/MeV )	Error ( Barn/MeV )
14. 60000	14. 40000	5. 50E-02	3. 80E-03	7. 60000	7. 40000	3. 02E-02	1. 09E-03
14. 40000	14. 20000	3. 28E-01	2. 52E-03	7. 40000	7. 20000	3. 36E-02	1. 12E-03
14. 20000	14. 00000	1. 27E+00	3. 74E-03	7. 20000	7. 00000	3. 44E-02	1. 13E-03
14. 00000	13. 80000	2. 62E+00	4. 65E-03	7. 00000	6. 80000	3. 79E-02	1. 11E-03
13. 80000	13. 60000	2. 67E+00	4. 44E-03	6. 80000	6. 60000	4. 24E-02	1. 11E-03
13. 60000	13. 40000	1. 58E+00	3. 31E-03	6. 60000	6. 40000	4. 52E-02	1. 11E-03
13. 40000	13. 20000	7. 94E-01	2. 37E-03	6. 40000	6. 20000	4. 68E-02	1. 12E-03
13. 20000	13. 00000	4. 68E-01	1. 93E-03	6. 20000	6. 00000	4. 93E-02	1. 13E-03
13. 00000	12. 80000	3. 00E-01	1. 71E-03	6. 00000	5. 80000	5. 11E-02	1. 15E-03
12. 80000	12. 60000	1. 88E-01	1. 54E-03	5. 80000	5. 60000	5. 32E-02	1. 16E-03
12. 60000	12. 40000	1. 19E-01	1. 41E-03	5. 60000	5. 40000	5. 48E-02	1. 17E-03
12. 40000	12. 20000	7. 97E-02	1. 38E-03	5. 40000	5. 20000	6. 07E-02	1. 19E-03
12. 20000	12. 00000	6. 39E-02	1. 31E-03	5. 20000	5. 00000	6. 68E-02	1. 21E-03
12. 00000	11. 80000	6. 52E-02	1. 31E-03	5. 00000	4. 80000	7. 48E-02	1. 23E-03
11. 80000	11. 60000	6. 89E-02	1. 31E-03	4. 80000	4. 60000	8. 54E-02	1. 25E-03
11. 60000	11. 40000	5. 92E-02	1. 27E-03	4. 60000	4. 40000	9. 57E-02	1. 27E-03
11. 40000	11. 20000	4. 96E-02	1. 21E-03	4. 40000	4. 20000	1. 06E-01	1. 29E-03
11. 20000	11. 00000	4. 94E-02	1. 17E-03	4. 20000	4. 00000	1. 14E-01	1. 32E-03
11. 00000	10. 80000	4. 82E-02	1. 16E-03	4. 00000	3. 80000	1. 28E-01	1. 36E-03
10. 80000	10. 60000	4. 19E-02	1. 12E-03	3. 80000	3. 60000	1. 46E-01	1. 40E-03
10. 60000	10. 40000	3. 77E-02	1. 11E-03	3. 60000	3. 40000	1. 62E-01	1. 45E-03
10. 40000	10. 20000	3. 35E-02	1. 08E-03	3. 40000	3. 20000	1. 91E-01	1. 51E-03
10. 20000	10. 00000	3. 03E-02	1. 10E-03	3. 20000	3. 00000	2. 26E-01	1. 61E-03
10. 00000	9. 80000	3. 18E-02	1. 12E-03	3. 00000	2. 80000	2. 61E-01	1. 71E-03
9. 80000	9. 60000	3. 32E-02	1. 12E-03	2. 80000	2. 60000	3. 05E-01	1. 80E-03
9. 60000	9. 40000	2. 95E-02	1. 11E-03	2. 60000	2. 40000	3. 66E-01	1. 98E-03
9. 40000	9. 20000	2. 30E-02	9. 49E-04	2. 40000	2. 20000	4. 45E-01	2. 13E-03
9. 20000	9. 00000	2. 26E-02	9. 35E-04	2. 20000	2. 00000	5. 34E-01	2. 36E-03
9. 00000	8. 80000	2. 22E-02	9. 41E-04	2. 00000	1. 80000	8. 48E-01	2. 63E-03
8. 80000	8. 60000	2. 49E-02	9. 78E-04	1. 80000	1. 60000	7. 53E-01	2. 85E-03
8. 60000	8. 40000	2. 63E-02	1. 00E-03	1. 60000	1. 40000	8. 73E-01	3. 41E-03
8. 40000	8. 20000	2. 59E-02	1. 03E-03	1. 40000	1. 20000	1. 00E+00	4. 14E-03
8. 20000	8. 00000	2. 55E-02	1. 05E-03	1. 20000	1. 00000	1. 15E+00	5. 77E-03
8. 00000	7. 80000	2. 79E-02	1. 07E-03	1. 00000	0. 80000	1. 28E+00	1. 29E-02
7. 80000	7. 60000	3. 02E-02	1. 09E-03				

data. Good agreements with experimental data are obtained, except for the (n,3n) process.

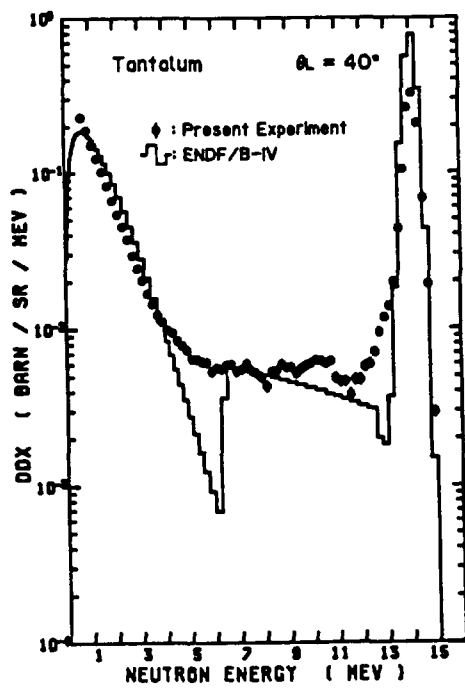
From these results, we can say that the present analysis with the EGNASH code is satisfactory and consistent to both of neutron and charged-particle emissions for the neutron-induced reaction of  $^{93}\text{Nb}$  at 14 MeV.

#### 4.2 Tantalum

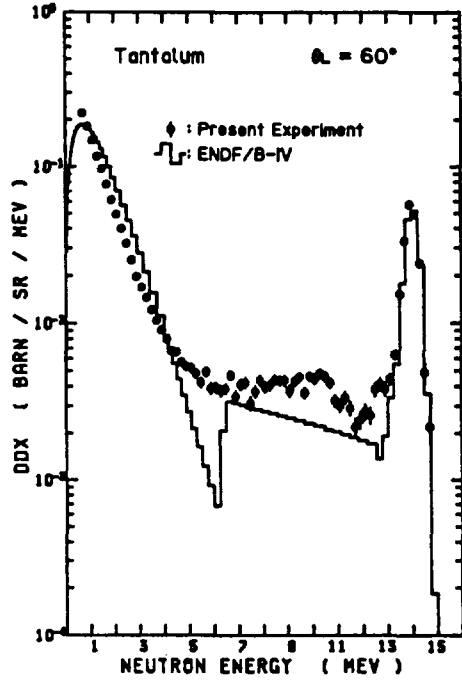
DDX : Measured double differential neutron emission cross sections are shown in Fig.11a through Fig.11h for 8 angles, i. e.,  $20^\circ$ ,  $40^\circ$ ,  $60^\circ$ ,  $80^\circ$ ,  $100^\circ$ ,  $120^\circ$ ,  $140^\circ$  and  $160^\circ$ , in comparison with the ENDF/B-IV data. The neutron emission



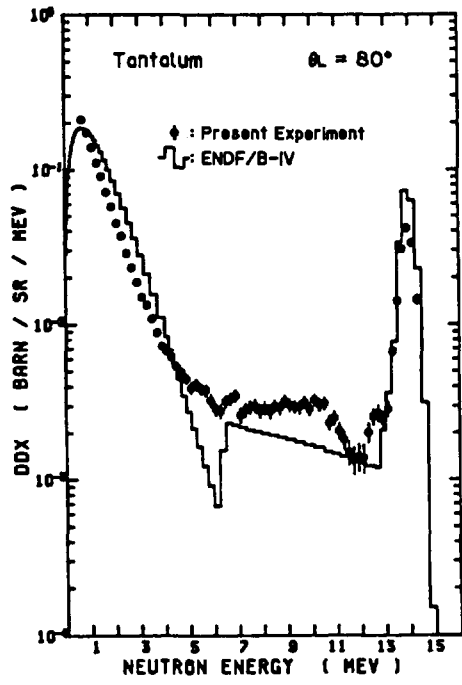
a)



b)

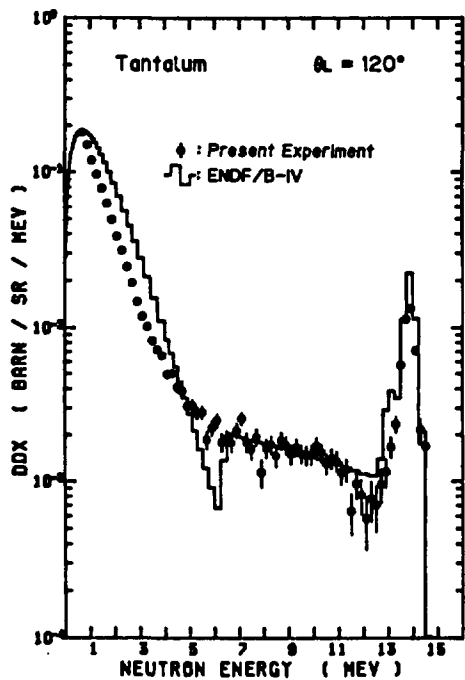
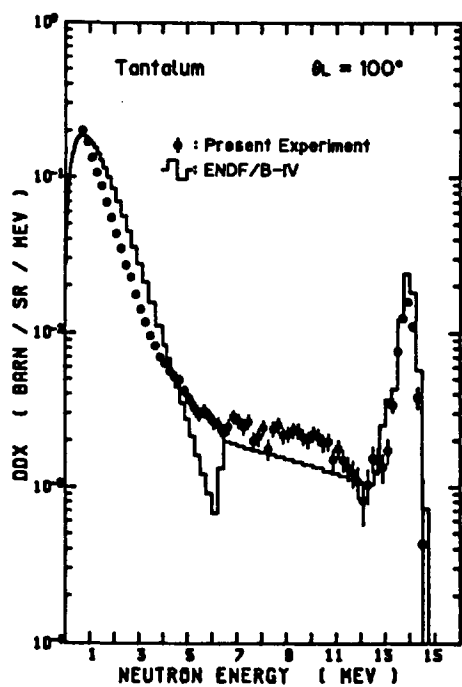


c)



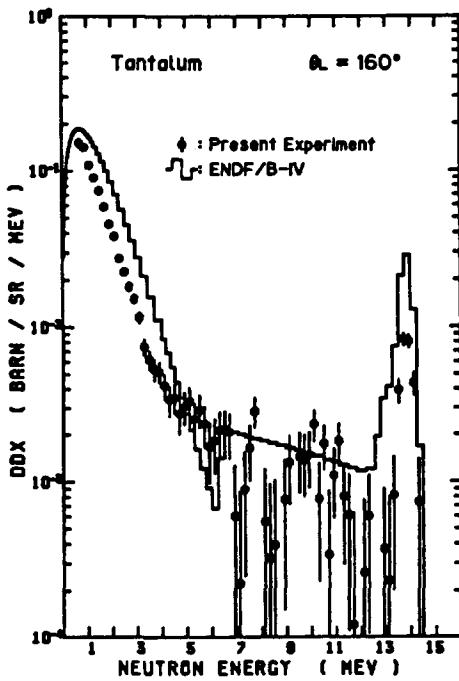
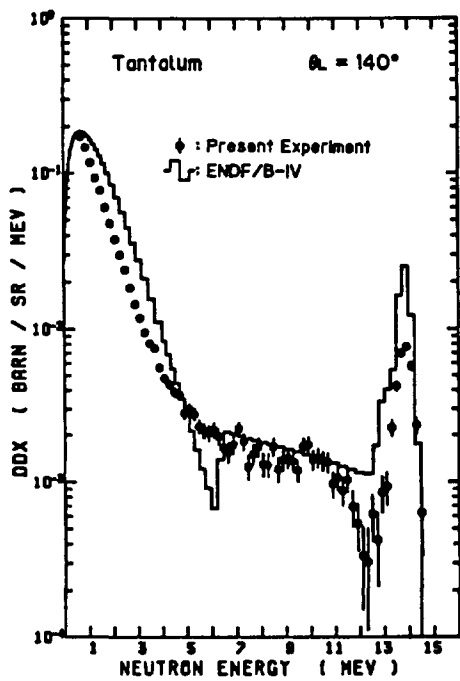
d)

Figs.11a-d Double differential neutron emission cross sections at 14.1 MeV for Ta-181, in comparison with ENDF/B-IV



e)

f)



g)

h)

Figs.11e-h Double differential neutron emission cross sections at 14.1 MeV for Ta-181, in comparison with ENDF/B-IV

Table-6-1

Tantalum partial differential cross sections at En=14.1 MeV

Angle (deg)	elastic		continuum		(n, 2n)	
	dσ/dΩ (b/sr)	error (b/sr)	dσ/dΩ (b/sr)	error (b/sr)	dσ/dΩ (b/sr)	error (b/sr)
1. 500E+01	3. 446E+00	6. 676E-03	7. 739E-02	1. 532E-03	3. 729E-01	5. 032E-03
2. 000E+01	1. 336E+00	3. 375E-03	5. 423E-02	1. 010E-03	3. 822E-01	3. 475E-03
3. 000E+01	1. 526E-01	8. 061E-04	3. 898E-02	5. 567E-04	3. 935E-01	1. 920E-03
4. 000E+01	2. 902E-01	9. 577E-04	3. 635E-02	3. 867E-04	3. 949E-01	1. 332E-03
5. 000E+01	1. 513E-01	7. 006E-04	3. 022E-02	3. 509E-04	3. 796E-01	1. 249E-03
6. 000E+01	3. 731E-02	4. 096E-04	2. 399E-02	3. 200E-04	3. 471E-01	1. 215E-03
7. 000E+01	4. 152E-02	5. 142E-04	2. 125E-02	3. 261E-04	3. 571E-01	1. 257E-03
8. 000E+01	3. 551E-02	4. 060E-04	1. 877E-02	3. 260E-04	3. 593E-01	1. 285E-03
9. 000E+01	1. 524E-02	2. 808E-04	1. 605E-02	3. 159E-04	3. 481E-01	1. 278E-03
1. 000E+02	1. 348E-02	2. 790E-04	1. 427E-02	3. 005E-04	3. 432E-01	1. 240E-03
1. 100E+02	1. 171E-02	2. 714E-04	1. 207E-02	2. 871E-04	3. 008E-01	1. 115E-03
1. 200E+02	9. 284E-03	1. 993E-04	1. 033E-02	2. 546E-04	2. 746E-01	1. 009E-03
1. 300E+02	5. 635E-03	1. 752E-04	9. 022E-03	2. 417E-04	2. 758E-01	9. 943E-04
1. 400E+02	7. 525E-03	2. 007E-04	9. 797E-03	2. 558E-04	2. 819E-01	1. 026E-03
1. 500E+02	8. 354E-03	2. 738E-04	8. 912E-03	4. 073E-04	2. 944E-01	1. 558E-03
1. 600E+02	6. 247E-03	4. 347E-04	7. 378E-03	7. 738E-04	2. 711E-01	2. 765E-03

spectra by ENDF/B-IV are approximately composed of 3 components, i. e., the elastic peak around 14 MeV, the continuum inelastic spectra in the 6-13 MeV region and the (n,2n) spectra in the lower energy region less than 6 MeV.

It is obvious that very artificial spectra are given in ENDF/B-IV for the continuum inelastic scattering, which generates non-physical gaps at around 6 MeV. In the energy region of 6-13 MeV, we can see 'structures' in the experimental spectra which may reflect significant contribution of direct inelastic scatterings with many discrete excited states. 'Bumps' around 10 MeV, corresponding to excitation energies around 4 MeV, should be notified. Additional peak near 13 MeV which we can see in the experimental data for 60° and 80° (from 30° to 90°, if we look through all the DDX data) may be due to excitations of low-lying states around 1 MeV in excitation energy. The continuum inelastic data given in ENDF/B-IV underestimate significantly the measured emission cross sections at forward angles, although agreements in magnitude are found at backward angles (120° and 140°).

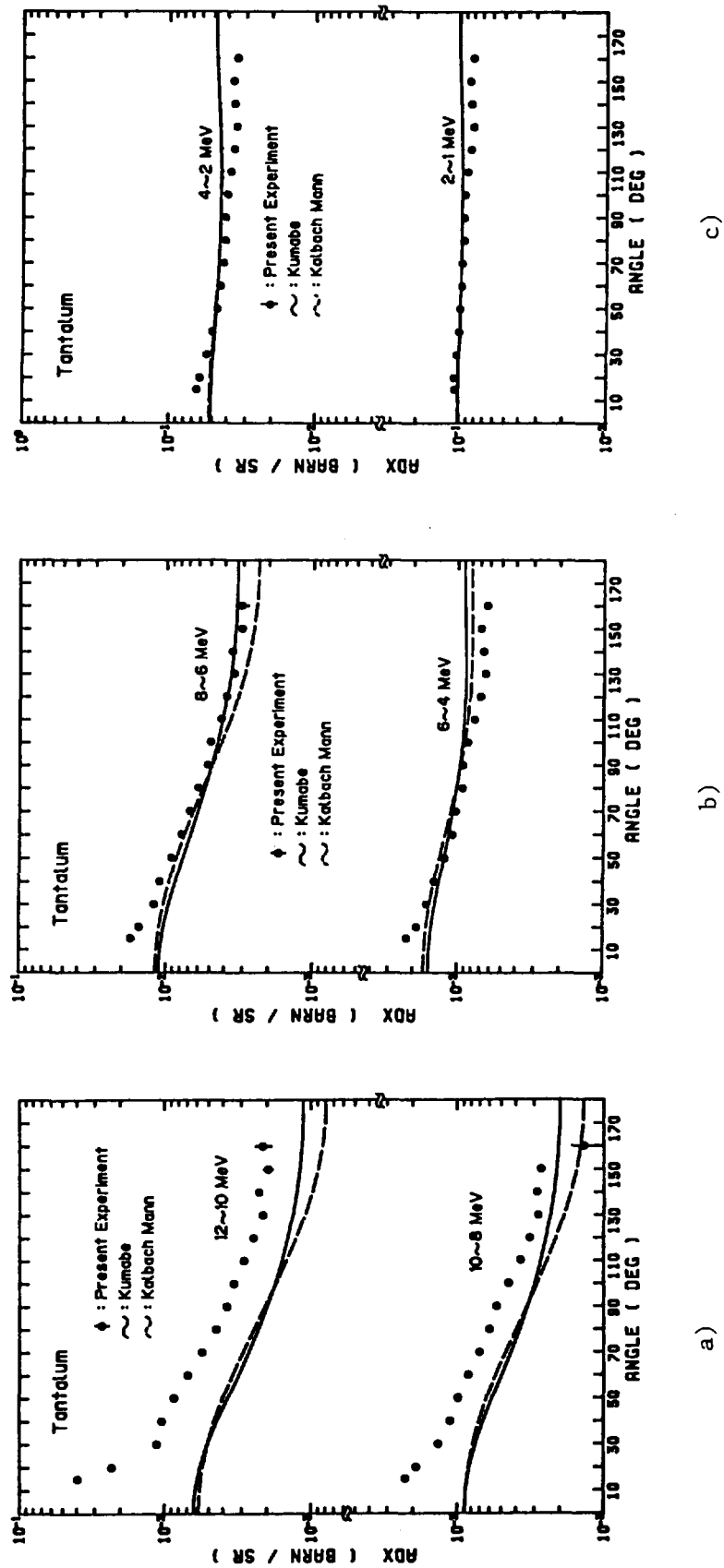
In the lower energy region less than 6 MeV where the  $^{181}\text{Ta}(n,2n)$  process becomes predominant, the ENDF/B-IV data show relatively good agreement at forward angles (20° and 40°), but significantly overestimate the experimental data at other angles (from 50° to 160°) in the 1-4 MeV region and give an evaporation-

Table-6-2

Tantalum integral of double differential cross section at En=14.1 MeV

Angle (deg)	12-10 MeV		10-8 MeV		8-6 MeV	
	d σ /dΩ (b/sr)	error (b/sr)	d σ /dΩ (b/sr)	error (b/sr)	d σ /dΩ (b/sr)	error (b/sr)
1. 500E+01	3. 940E-02	7. 237E-04	2. 255E-02	5. 840E-04	1. 728E-02	5. 981E-04
2. 000E+01	2. 287E-02	4. 617E-04	1. 905E-02	3. 966E-04	1. 504E-02	4. 011E-04
3. 000E+01	1. 126E-02	2. 154E-04	1. 340E-02	2. 041E-04	1. 190E-02	2. 083E-04
4. 000E+01	1. 036E-02	1. 398E-04	1. 114E-02	1. 352E-04	1. 092E-02	1. 402E-04
5. 000E+01	8. 521E-03	1. 306E-04	9. 805E-03	1. 303E-04	9. 146E-03	1. 357E-04
6. 000E+01	6. 911E-03	1. 311E-04	8. 379E-03	1. 339E-04	7. 807E-03	1. 411E-04
7. 000E+01	5. 507E-03	1. 341E-04	6. 983E-03	1. 386E-04	6. 845E-03	1. 479E-04
8. 000E+01	4. 430E-03	1. 394E-04	5. 982E-03	1. 470E-04	5. 983E-03	1. 564E-04
9. 000E+01	3. 754E-03	1. 511E-04	5. 358E-03	1. 608E-04	5. 179E-03	1. 691E-04
1. 000E+02	3. 367E-03	1. 276E-04	4. 455E-03	1. 373E-04	4. 946E-03	1. 493E-04
1. 100E+02	2. 878E-03	1. 075E-04	3. 702E-03	1. 177E-04	4. 203E-03	1. 296E-04
1. 200E+02	2. 469E-03	9. 054E-05	3. 203E-03	1. 014E-04	3. 914E-03	1. 125E-04
1. 300E+02	2. 140E-03	8. 102E-05	2. 809E-03	9. 144E-05	3. 464E-03	1. 008E-04
1. 400E+02	2. 280E-03	8. 140E-05	2. 865E-03	9. 129E-05	3. 567E-03	9. 909E-05
1. 500E+02	1. 969E-03	1. 273E-04	2. 694E-03	1. 443E-04	3. 084E-03	1. 534E-04
1. 600E+02	2. 138E-03	2. 472E-04	1. 374E-03	2. 820E-04	3. 093E-03	2. 968E-04

Angle (deg)	6-4 MeV		4-2 MeV		2-1 MeV	
	d σ /dΩ (b/sr)	error (b/sr)	d σ /dΩ (b/sr)	error (b/sr)	d σ /dΩ (b/sr)	error (b/sr)
1. 500E+01	2. 202E-02	6. 372E-04	6. 392E-02	8. 631E-04	1. 075E-01	1. 121E-03
2. 000E+01	1. 879E-02	4. 268E-04	6. 097E-02	5. 978E-04	1. 078E-01	7. 942E-04
3. 000E+01	1. 610E-02	2. 256E-04	5. 451E-02	3. 324E-04	1. 039E-01	4. 619E-04
4. 000E+01	1. 429E-02	1. 523E-04	5. 023E-02	2. 334E-04	1. 005E-01	3. 359E-04
5. 000E+01	1. 227E-02	1. 495E-04	4. 652E-02	2. 315E-04	9. 897E-02	3. 370E-04
6. 000E+01	1. 082E-02	1. 565E-04	4. 420E-02	2. 424E-04	9. 644E-02	3. 509E-04
7. 000E+01	1. 028E-02	1. 648E-04	4. 226E-02	2. 517E-04	9. 563E-02	3. 628E-04
8. 000E+01	9. 268E-03	1. 729E-04	4. 107E-02	2. 620E-04	9. 295E-02	3. 713E-04
9. 000E+01	9. 145E-03	1. 873E-04	4. 120E-02	2. 779E-04	9. 306E-02	3. 867E-04
1. 000E+02	8. 529E-03	1. 676E-04	4. 001E-02	2. 546E-04	9. 179E-02	3. 627E-04
1. 100E+02	7. 657E-03	1. 481E-04	3. 827E-02	2. 306E-04	8. 889E-02	3. 356E-04
1. 200E+02	7. 019E-03	1. 296E-04	3. 622E-02	2. 047E-04	8. 462E-02	3. 035E-04
1. 300E+02	6. 496E-03	1. 170E-04	3. 489E-02	1. 874E-04	8. 112E-02	2. 812E-04
1. 400E+02	6. 694E-03	1. 146E-04	3. 602E-02	1. 839E-04	8. 397E-02	2. 792E-04
1. 500E+02	6. 938E-03	1. 761E-04	3. 649E-02	2. 662E-04	8. 568E-02	3. 910E-04
1. 600E+02	6. 319E-03	3. 308E-04	3. 438E-02	4. 625E-04	8. 127E-02	6. 381E-04



Figs. 12a-c Angular distributions of  $^{181}\text{Ta}$  neutron emission cross sections at 14.1 MeV, for selected energy-bins, in comparison with EGNASH calculations using the Kalbach-Mann or the Kumabe's systematics for preequilibrium and equilibrium processes

like spectral shape which is different from the experimental one especially in the 3-6 MeV region where the contribution of preequilibrium process is foreseen.

ADX : Angular distributions of neutron emission cross sections for artificial energy-bins, i. e., 12-10, 10-8, 8-6, 6-4, 4-2 and 2-1 MeV, are shown in Figs. 12a, 12b and 12c, in comparison with the EGNASH calculations. For energy-bins lower than 8 MeV, the EGNASH calculations show relatively good agreements with the experiments although the experiments show slightly more enhancement of neutron emission in forward angles. The Kumabe's systematics agrees better than the Kalbach-Mann's for the 8-6 MeV bin, at backward angles, but the situation is reversed for the 6-4 MeV bin. For the 12-10 and 10-8 MeV bins, angular dependences of the calculations resemble to experimental ones, but the magnitudes are much smaller since the contribution of direct processes is not included in the calculations.

Differential elastic scattering cross sections are shown in Fig.13. Good agreement with the ENDF/B-IV data are seen. In Fig.14, integrated emission cross sections for the 'continuum' of 6-13 MeV range and the  $(n,2n)$  components of 0-6 MeV range are shown in comparison with the ENDF/B-IV data. To obtain  $^{181}\text{Ta}(n,2n)$  angular differential cross sections, the low energy part (less than about 3 MeV) of measured DDX spectrum was fit to the Maxwellian distribution to make interpolation to zero energy and DDX data were integrated over the 0-6 MeV region. The experimental angular distribution of  $^{181}\text{Ta}(n,2n)$  cross sections shows slight enhancement of neutron emission in forward angles, compared with isotropic distribution of the ENDF/B-IV data. This angular dependence may be due to the inclusion of preequilibrium components in the experimental data. By integrating this angular distribution, the  $^{181}\text{Ta}(n,2n)$  cross section at 14.1 MeV was reduced to be  $2.10 \pm 0.08$  barn which agree very well with the result of the EGNASH calculation and other experiments<sup>14</sup> as shown in Fig.15.

EDX : Angle -integrated neutron emission spectra for  $^{181}\text{Ta}$  are shown in Figs. 16a and 16b. In Fig.16a, the measured EDX data are compared with the Pavlik-Vonach evaluation<sup>5</sup> and the ENDF/B-IV data. In the 2-6 MeV region, the present experimental data are significantly smaller, about 30 % at 4 MeV, than the Pavlik-Vonach curve. Disagreement with the ENDF/B-IV data is obvious in the whole energy region because of difference in spectral patterns.

In Fig.16b, comparison is made with the EGNASH calculations. In the energy region less than about 6 MeV, very good agreement with the experiment is obtained. The preequilibrium component is dominant in the 4-8 MeV region. Although a significant contribution of preequilibrium process is calculated in the 6-11 MeV region, the differences between the 'higher' experimental points and the 'lower'

Fig.15  $^{181}\text{Ta}(n,2n)$  and  $^{181}\text{Ta}(n,3n)$  cross sections, compared with the present EGNASH calculations (solid and broken)

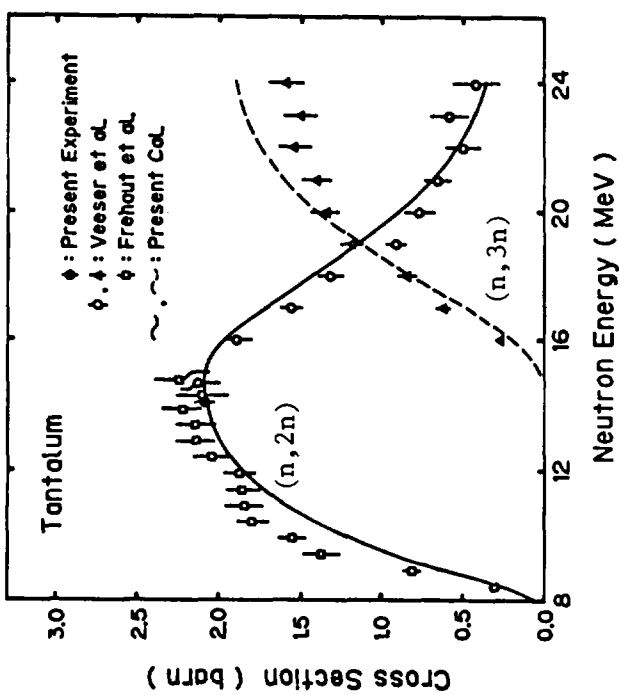
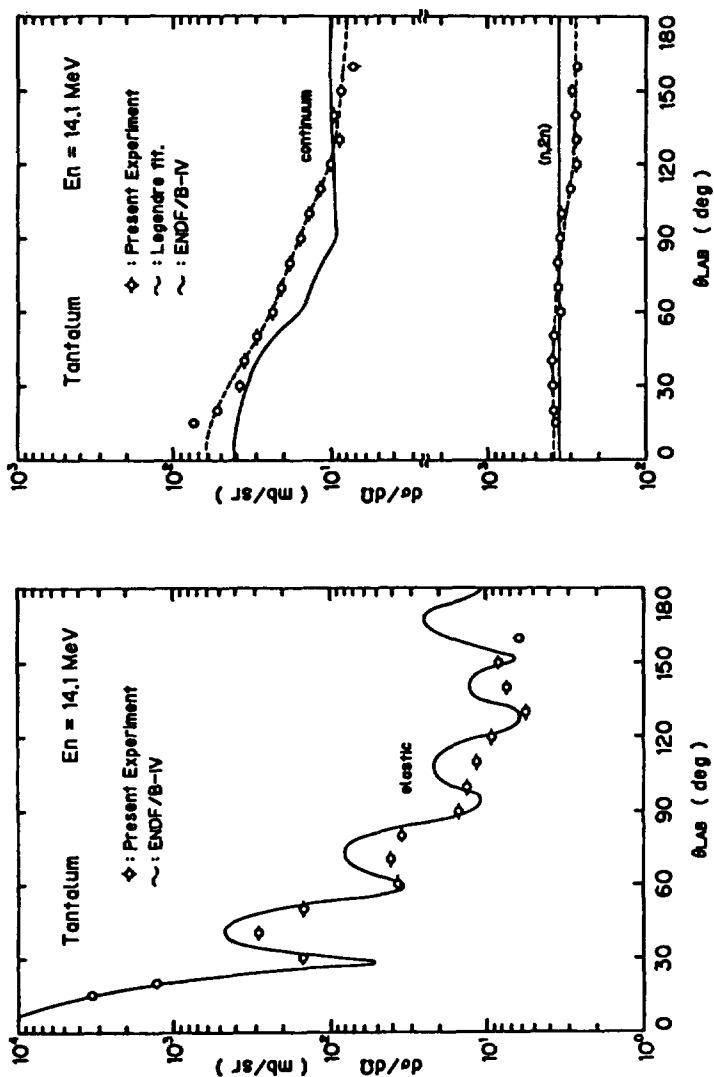


Fig.13 Differential elastic scattering cross sections for  $^{181}\text{Ta}$  (n,2n) cross sections, for Ta-181



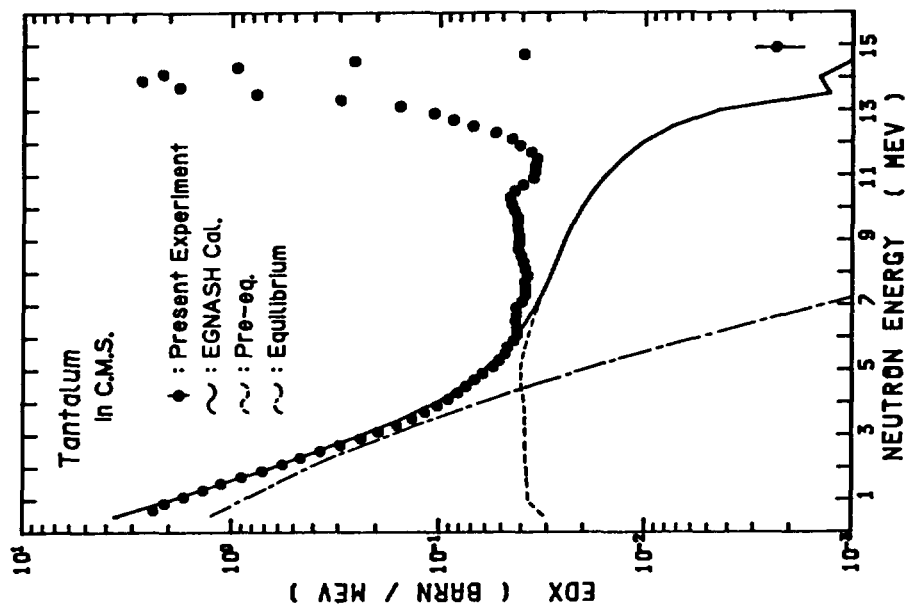


Fig.16b Angle-integrated neutron emission spectra for Ta-181, at  $E_n = 14.1$  MeV, in comparison with EGNASH calculations

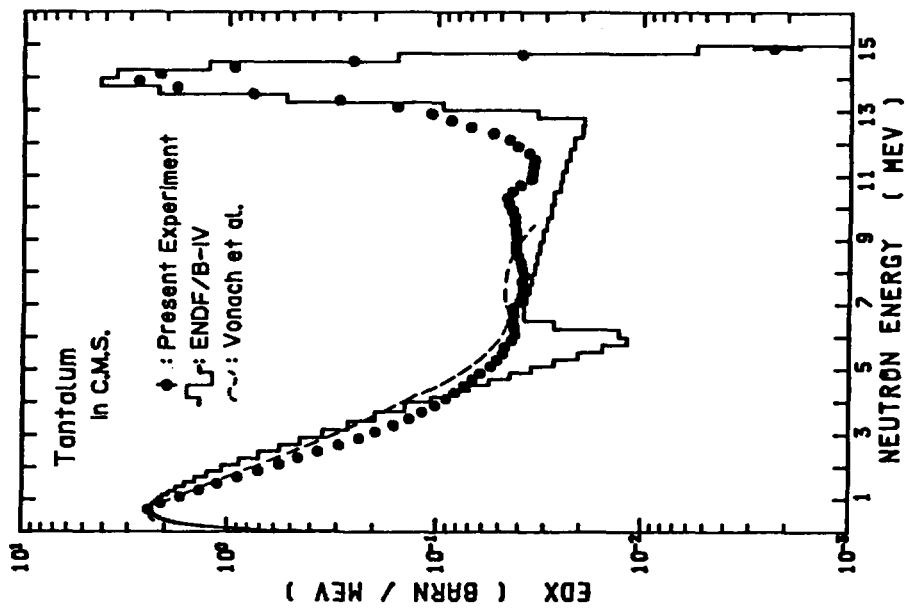


Fig.16a Angle-integrated neutron emission spectra for Ta-181, in comparison with the Pavlik-Vonach evaluation (broken) and the ENDF/B-IV data (histogram), at  $E_n = 14.1$  MeV

Table-7

Tantalum secondary neutron emission spectrum at En=14.1 MeV

E-upper ( MeV )	E-lower ( MeV )	DATA ( Barn/MeV )	Error ( Barn/MeV )	E-upper ( MeV )	E-lower ( MeV )	DATA ( Barn/MeV )	Error ( Barn/MeV )
15.00000	14.80000	2.34E-03	5.99E-04	7.80000	7.60000	3.88E-02	8.10E-04
14.80000	14.60000	3.91E-02	9.75E-04	7.60000	7.40000	3.85E-02	8.09E-04
14.60000	14.40000	2.54E-01	1.68E-03	7.40000	7.20000	3.87E-02	8.18E-04
14.40000	14.20000	8.43E-01	2.48E-03	7.20000	7.00000	3.99E-02	8.14E-04
14.20000	14.00000	2.16E+00	3.33E-03	7.00000	6.80000	4.26E-02	8.03E-04
14.00000	13.80000	2.73E+00	3.77E-03	6.80000	6.60000	4.23E-02	8.00E-04
13.80000	13.60000	1.80E+00	3.16E-03	6.60000	6.40000	4.27E-02	8.08E-04
13.60000	13.40000	7.68E-01	2.18E-03	6.40000	6.20000	4.22E-02	8.13E-04
13.40000	13.20000	2.97E-01	1.49E-03	6.20000	6.00000	4.19E-02	8.24E-04
13.20000	13.00000	1.55E-01	1.19E-03	6.00000	5.80000	4.36E-02	8.32E-04
13.00000	12.80000	1.07E-01	1.05E-03	5.80000	5.60000	4.69E-02	8.53E-04
12.80000	12.60000	8.66E-02	9.85E-04	5.60000	5.40000	4.82E-02	8.63E-04
12.60000	12.40000	6.94E-02	9.37E-04	5.40000	5.20000	5.15E-02	8.78E-04
12.40000	12.20000	5.40E-02	8.87E-04	5.20000	5.00000	5.52E-02	8.84E-04
12.20000	12.00000	4.48E-02	8.48E-04	5.00000	4.80000	6.17E-02	9.01E-04
12.00000	11.80000	4.09E-02	8.22E-04	4.80000	4.60000	6.77E-02	9.14E-04
11.80000	11.60000	3.61E-02	7.94E-04	4.60000	4.40000	7.45E-02	9.28E-04
11.60000	11.40000	3.39E-02	7.70E-04	4.40000	4.20000	8.19E-02	9.52E-04
11.40000	11.20000	3.44E-02	7.54E-04	4.20000	4.00000	9.08E-02	9.78E-04
11.20000	11.00000	3.47E-02	7.32E-04	4.00000	3.80000	1.02E-01	1.01E-03
11.00000	10.80000	3.52E-02	7.21E-04	3.80000	3.60000	1.17E-01	1.05E-03
10.80000	10.60000	3.96E-02	7.27E-04	3.60000	3.40000	1.35E-01	1.08E-03
10.60000	10.40000	4.34E-02	7.39E-04	3.40000	3.20000	1.61E-01	1.14E-03
10.40000	10.20000	4.59E-02	7.43E-04	3.20000	3.00000	1.96E-01	1.21E-03
10.20000	10.00000	4.51E-02	7.43E-04	3.00000	2.80000	2.36E-01	1.30E-03
10.00000	9.80000	4.36E-02	7.43E-04	2.80000	2.60000	2.95E-01	1.42E-03
9.80000	9.60000	4.23E-02	7.43E-04	2.60000	2.40000	3.70E-01	1.59E-03
9.80000	9.40000	4.20E-02	7.50E-04	2.40000	2.20000	4.63E-01	1.67E-03
9.40000	9.20000	4.15E-02	7.57E-04	2.20000	2.00000	5.70E-01	1.80E-03
9.20000	9.00000	4.12E-02	7.56E-04	2.00000	1.80000	7.16E-01	1.99E-03
9.00000	8.80000	4.13E-02	7.65E-04	1.80000	1.60000	8.99E-01	2.25E-03
8.80000	8.60000	4.16E-02	7.71E-04	1.60000	1.40000	1.12E+00	2.58E-03
8.60000	8.40000	4.03E-02	7.79E-04	1.40000	1.20000	1.37E+00	2.93E-03
8.40000	8.20000	3.93E-02	7.88E-04	1.20000	1.00000	1.68E+00	3.60E-03
8.20000	8.00000	3.86E-02	7.97E-04	1.00000	0.80000	2.10E+00	5.29E-03
8.00000	7.80000	3.76E-02	8.00E-04	0.80000	0.60000	2.39E+00	1.25E-02

calculated curve should show the contribution of direct reaction processes which is not included in the present EGNASH calculation. A similar result is obtained<sup>15</sup> for the case of <sup>209</sup>Bi, where two distinct peaks of direct reactions (2.68 and 4.28 MeV states) are observed in the experimental angle-integrated spectrum. In the case of <sup>181</sup>Ta, however, the measured spectrum in the 6-13 MeV region is rather 'monotonous', although a 'bump' is seen at about 10 MeV. These facts tell us that so many discrete states are directly excited with comparable magnitudes in this energy region, for <sup>181</sup>Ta. The present experiment has not been able to resolve these many discrete states. To analyse with the DWUCK4 calculation,

discrete level data upto about 7 MeV in excitation energy are needed, however not available at the moment. We might use rough approximation of several 'pseudo-discrete levels' for engineering purpose to meet a considerable agreement with the experiment. It is however expected that 'much-higher' resolution experiments will be conducted in future to resolve these.

### 5. Conclusions

A relatively high-resolution TOF experiment was undertaken to measure double differential neutron emission cross sections at the incident neutron energy of 14.1 MeV, for  $^{93}\text{Nb}$  and  $^{181}\text{Ta}$ . Angular differential cross sections for resolved levels and angle-integrated neutron emission spectra were reduced from measured DDX data.

Using the EGNASH code (ELIESE-GNASH joint program), theoretical analyses were done taking into account contributions of direct, preequilibrium and equilibrium processes for  $^{93}\text{Nb}$ , and of preequilibrium and equilibrium processes for  $^{181}\text{Ta}$ .

For  $^{93}\text{Nb}$ , very good agreements between experiments and calculations were obtained for DDX data by using the Kalbach-Mann type systematics for preequilibrium and equilibrium angular distributions and the DWBA calculations with DWUCK4. Agreement was also excellent for angle-integrated emission spectra, while the Pavlik-Vonach evaluation curve drew high in the 3-6 MeV region.

For  $^{181}\text{Ta}$ , the EGNASH calculation without direct components could very well reproduce experimental neutron emission spectra and angular dependencies in the 1-8 MeV region, while it was concluded that direct reaction processes for many discrete excited states (upto about 7 MeV in excitation energy) could significantly contribute in the 6-13 MeV region although the preequilibrium process could be comparable to the direct process in the 6-11 MeV region. High resolution experiments will be further expected for  $^{181}\text{Ta}$ .

### Acknowledgment

The authors are grateful to Dr. N. Yamamuro (Professor emeritus of the Tokyo Institute of Technology) for providing them the EGNASH code.

## References

- 1) Report of Working Group II (chaired by H. Vonach), IAEA Specialist Meet., Rome, Italy, Nov. 17-19, 1986
- 2) A. Takahashi, et al., J. Nucl. Sci. Tech., 25, 215-232 (1988)
- 3) N. Yamamuro, 'Nuclear Cross Section Calculations with a Simplified Input Version of ELISE-GNASH Joint Program', Int. Conf. Nuclear Data, Mito, Japan, May 1988 (Proc. to be published)
- 4) ENDF/B-IV Summary Documentation, BNL-NCS 17451 (1975)
- 5) A. Pavlik, H. Vonach, ISSN 0344-8401, Fachinformationszentrum Karlsruhe No. 13-4 (1988)
- 6) E. Ichimura, A. Takahashi, OKTAVIAN Rep. A-87-02, Osaka Univ. (1987)
- 7) A. Takahashi, et al., JAERI-M 88-065, pp.279-318 (1988)
- 8) P. D. Kunz, 'Distorted Wave Code DWUCK4', Univ. Colorado (1974)
- 9) C. Kalbach, F. M. G. Mann, Phys. Rev., C23, 112 (1981)
- 10) H. Kalka, et al., Zeitschrift f. Physik A, 329, 331 (1988)
- 11) R. L. Walter, P. P. Guss, Proc. Conf. Nucl. Data for Basic and Appl. Sci., Santa Fe, 13-17 May 1985, Vol.2, 1079, Gordon and Breach Sci. Publ. (1986)
- 12) I. Kumabe, et al., private communication (1988)
- 13) N. Yamamuro, JAERI-M 88-140 (1988)
- 14) CINDA 82 and CINDA 84, IAEA
- 15) A. Takahashi, et al., JAERI-M 88-102 (1988)